InAs Quantum Dot Arrays Decorating the Facets of GaAs Nanowires

Emanuele Uccelli,[†,‡,¶] Jordi Arbiol,[§,¶] Joan Ramon Morante,[⊥,‖] and Anna Fontcuberta i Morral[†,‡,*]

[†]Laboratoire des Matériaux Semiconducteurs, Ecole Polytechnique Fédérale de Lausanne, CH-1015 Lausanne, Switzerland, [‡]Walter Schottky Institut and Physics Department, am Coulombwall 3, D-85748 Garching, Germany, [§]Institució Catalana de Recerca i Estudis Avançats (ICREA) and Institut de Ciència de Materials de Barcelona, CSIC, E-08193 Bellaterra, CAT, Spain, [⊥]Departament d'Electrònica, Universitat de Barcelona, E-08028 Barcelona, CAT, Spain, and [‖]Catalonia Institute for Energy Research (IREC), E-08019 Barcelona, CAT, Spain. [¶]These authors contributed equally to this work.

ABSTRACT InAs quantum dot arrays are obtained on GaAs nanowire facets by molecular beam epitaxy. The GaAs nanowires are first grown by the gallium-assisted catalyst-free method. Decoration of the nanowire facets with InAs quantum dots is achieved only when the facets are capped with an ultrathin AlAs layer, as demonstrated by atomic force, high-resolution electron microscopy, and energy-dispersive X-ray spectroscopy line scans. The excitation of single and double excitons in the quantum dots are demonstrated by low-temperature photoluminescence spectroscopy realized on the single nanowires. This new type of heterostructures opens a new avenue to the fabrication of highly efficient single-photon sources, novel quantum optics experiments, as well as the realization of intermediate-band nanowire solar cells for third-generation photovoltaics.

KEYWORDS: nanowires · quantum dots · optical properties · solar cells · epitaxy

Semiconductor nanowires are building blocks for future generations of devices in manifold areas such as single-molecule sensing,[1,2] functional nanoelectronic devices,[3,4] high-mobility field effect transistors,[5] batteries,[6,7] solar cells,[8,9] and thermoelectric devices.[10,11] At the same time, they have provided a fruitful soil for the study of quantum mechanics related phenomena that could lead to applications in emerging fields such as quantum information and technology.[12−15] For this to become a reality, the mastering of the nanowire morphology, composition, and structure has been shown to be key factor.[16] Furthermore, the formation of heterostructures within the nanowire and/or the combination of nanowires with other nanostructures adds advanced functionalities.[3,17]

The particular geometry of nanowires has enabled optical experiments that were unthought of with classical thin film structures. For example, if thick enough, they can act as extremely small waveguides.[18,19] If thin enough, the light emission is extremely bright thanks to the suppression of total internal reflection.[20] As a consequence, they are currently considered as ideal elements for ultrabright light-emitting diodes (LEDs) and single-photon sources.[21−23] By inserting quantum dot (QD) structures in the nanowire waveguides, the brightness of the QD can be increased up to an order of magnitude higher compared to a self-assembled QD on a planar substrate. Finally, QDs could be embedded in the intrinsic region of radial p-i-n devices to optimize the absorption in nanowire-based solar cells.[24−26]

Nanowires are typically obtained by the vapor−liquid−solid (VLS) method,[27] in which gold nanoparticles preferentially gather and catalyze the growth precursors leading to the precipitation of solid nanowires underneath. By varying the composition of the precursors, it is possible to vary the composition in the axial direction and to form axial heterostructures.[17,28−30] In the case where the length of the axial junction is of the order of few nanometers, quantization effects are observed due to the formation of quantum dot structures.[31] At this point, the abruptness of the interface between the junctions is a critical parameter. In the VLS growth mode, the temporal response of switching the composition of the catalyst droplet is the key factor for making feasible a nanowire axial heterostructure with sharp interfaces.[32,33] Additionally, it has been found that it is not always a straightforward process to change the composition in a nanowire from A to B and back to A. It has been shown that interface energy phenomena can lead to the kinking of the nanowire when switching from B to A.[34] All of these are unique phenomena in the nanowire geometry or growth modus. These challenges could be circumvented by adopting the typical thin film strategy of self-assembled Stranski-Krastanov QD growth.[35] Planar Stranski-Krastanov QDs have excellent optical properties and have

*Address correspondence to anna.fontcuberta-morral@epfl.ch.

Received for review May 1, 2010 and accepted September 03, 2010.

Published online September 14, 2010.
10.1021/nn101604k

© 2010 American Chemical Society

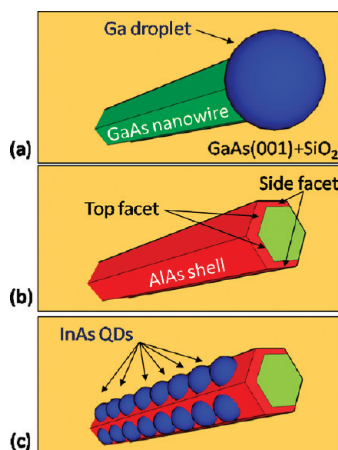

Figure 1. Schematics of the fabrication of the nanowire heterostructures: (a) GaAs nanowire growth on a GaAs (001)-oriented substrate. The nanowires nucleate below a Ga droplet, 35° tilted respect with the surface. (b) Switching from axial to radial growth by changing to As-rich conditions. Epitaxial growth takes place on the nanowire side facets, forming a shell. (c) Radial growth of InAs QDs can only be obtained if an AlAs shell layer has been previously deposited.

enabled the progress of many solid state applications such as single-photon emission, light-emitting diodes, memories, and multicarrier solar cells. To our knowledge, no Stranski-Krastanov growth of III−V QDs has been realized on the facets of nanowires, although some attempts have been realized.[36] As a consequence of the nanowire geometry, self-assembled QDs can only easily be obtained directly on the facets, which typically belong to either the {110} or the {112} crystal families. In the case of catalyst-free gallium-assisted grown GaAs nanowires, the facets always belong to the {110} family,[37,38] while in the case of gold-catalyzed nanowires, the facets tend to belong to the {112} family,[39] though there are some exceptions.[40] Self-assembled InAs QDs are typically grown on (001) GaAs surfaces.[41,42] Due to a nonfavorable surface energy of {110} surfaces, InAs QDs do not form on GaAs (110)-oriented surfaces.[43,44] Instead, micrometer-sized triangular structures full of dislocations are observed.[45] Nevertheless, it has been recently demonstrated that {110} surfaces can be rendered favorable to the formation of InAs QDs by previously depositing a thin AlAs layer.[46−49] Such a strategy used in classical 2D epitaxy should be applicable to the nanowire geometry. In this paper, we demonstrate that self-assembly of Stranski-Krastanov QDs is possible on the nanowire facets. Such a method allows circumventing the intrinsic limitations of the VLS growth mode for QD formation.

The nanowire heterostructures were obtained, as schematized in Figure 1. First, GaAs nanowires were grown by the gallium-assisted catalyst-free method as described elsewhere.[50,51] Then, the axial growth was stopped to continue with direct epitaxy on the facets. The main characteristics of this type of synthesis include the following: (i) the nanowires are formed under gallium-rich conditions, in which a Ga droplet acts as a seed; (ii) the growth axis coincides with the [111]B direction; (iii) the nanowires present a hexagonal prism morphology, with the facets pertaining to the {110} family; and (iv) it is possible to switch from axial to radial growth and deposit layers epitaxially on the facets to form core−shell heterostructures by increasing the As_4 pressure up to 5×10^{-5} mbar and by lowering the temperature from 630 down to 450 °C.[37,38]

TABLE 1. Description of the Three Types of Samples Fabricated[a]

	core	shell		
	GaAs	AlAs	InAs	GaAs
sample I	2 μm		5 ML (1.5 ML)	
sample II	2 μm	5 nm (1.5 nm)	5 ML (1.5 ML)	
sample IIc	2 μm	5 nm (1.5 nm)	5 ML (1.5 ML)	15 nm (4.5 nm)
sample IIIc	4 μm	5 nm (1.5 nm)	1.25 ML (0.4 ML)	15 nm (4.5 nm)

[a]The thickness of AlAs, InAs, and GaAs deposited on the top facets is shown. The thickness in parentheses corresponds to the thickness deposited on the lateral facets. For InAs, we report the value in monolayers, as this is what is usually reported in Stranski-Krastanov type of growth.

In order to demonstrate how InAs QDs can be obtained to decorate the nanowire facets, three types of samples were fabricated. For clarity, the conditions are shown in Table 1. The core of all structures consisted of 2−4 μm long GaAs nanowires, grown on (001) or (111)B GaAs substrates. Samples I−III exhibited different materials deposited on the side facets. One should note here that the nanowires were tilted 35° with respect to the nanowire surface. As a result, the thickness obtained in each of the facets depended on the relative position with respect to the incoming flow, the two top facets receiving the highest amount of material (50%).[38] Sample I was achieved by directly growing nominally 5 monolayers (ML) of InAs on the nanowire top side facets. In samples II and III, a nominally 5 nm thick AlAs layer was inserted prior to the growth of 5 and 1.25 ML InAs, respectively. Finally, the suffix "c" corresponds to samples that have been capped with GaAs to avoid the oxidation of InAs and enable the investigation of the optical properties.

The morphology of the three types of samples was studied both by atomic force microscopy (AFM) and transmission electron microscopy (TEM). For the AFM measurements, the nanowires were mechanically transferred to a silicon substrate. In Figure 2, the typical AFM measurements of a bare nanowire and samples I and II are shown. The bare nanowire presents a prismatic morphology, with the top facet being parallel to the substrate surface. The surface roughness is extremely low, at least below 0.7 nm. Samples I and II present a quite different geometry from the bare nanowire. For sample I, we observe the presence of a large trapezoidal structure in the middle of the nanowire trunk (Figure 2b). The size of this structure extends up to a few hundred nanometers in length, and it has a

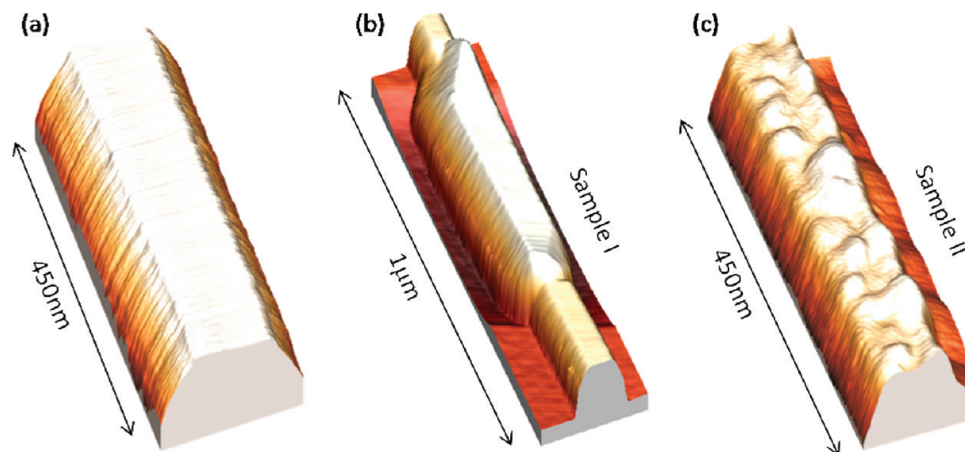

Figure 2. Atomic force microscopy measurements of three different GaAs nanowire structures: (a) GaAs nanowire, (b) sample I corresponding to the direct growth of 5 ML of InAs on the top facets, and (c) sample II corresponding to the deposition of the same amount of InAs on top of a thin AlAs shell, leading to the formation of QD arrays.

height of few tens of nanometers. Such a morphology is strongly reminiscent of the defects formed when InAs is grown directly on {110} GaAs surfaces.[43] Several of these structures are randomly found along the nanowire axis, suggesting that In adatoms strongly diffuse along the nanowire facets before they precipitate in the most energetically stable structure.[52] Sample II exhibits a quite different morphology from the two previous samples. When an AlAs layer is deposited prior to the InAs, QDs appear on the nanowire facets (Figure 2c). They exhibit the typical dimensions of Stranski-Krastanov QDs: a few nanometers high and up to few tens of nanometers in length. Interestingly, the QDs are aligned in a chain-like configuration along the AlAs facet. Formation of both single and double rows of QDs has been observed.

In order to demonstrate the composition of the QDs, we performed a scanning transmission electron microscopy (STEM) analysis in high angular annular dark field (HAADF) mode together with energy-dispersive X-ray spectroscopy (EDX) line scans (Figure 3).[53] Due to the higher *Z* of In with respect to Al and Ga, the InAs QD shown in Figure 3 is observed with a brighter intensity (HAADF mode). The EDX line scan obtained along the nanowire width (dashed line) also shows a clear increase of the In and a decrease of the Ga signals when approaching the QD protrusion. These measurements clearly confirm that the QDs are formed by InAs.

In order to have a more complete view of these structures, samples I, II, and III were investigated by high-resolution transmission electron microscopy (HRTEM). A typical TEM micrograph of sample II is shown in Figure 4a. There, the formation of small triangular QD-like objects at the nanowire surface is observed. In Figure 4b, a high-resolution image is shown. The obtained image is compatible with the formation of a truncated pyramid, a few nanometers in height and ~15 nm in length. The HRTEM micrograph in Figure 4b also shows the presence of the AlAs layer between the InAs dot and the GaAs nanowire. Interestingly, some interference fringes appear just below the InAs QD (see a magnified image of the overlapping fringes in Figure 4b, bottom inset). These interferences are in good agreement with a model where the QD would be partially buried in the AlAs shell layer. Only cross-section HRTEM analysis can confirm this, as it will be shown in the following. In the meanwhile, the high-resolution analysis indicates that there is an epitaxial relation with the core. The power spectrum obtained on the image (Figure 4c) shows the splitting of the {111} and {002} spots according to the expected mismatches occurring between the three binary materials. The bulk cell parameters of these three binary semiconductors are 0.5654, 0.5620, and 0.6058 nm for GaAs, AlAs, and InAs, respectively. The expected interplanar distances for the observed {111} planes should be 0.3264, 0.3245, and 0.3498 nm for GaAs, AlAs, and InAs, respectively. There should be a lattice mismatch of −0.6% between AlAs and GaAs and 7.2% between InAs and GaAs. The small mismatch between AlAs and GaAs can be visualized in the power spectrum, as both spots are almost overlapped (see top right inset). In the case of InAs, the corresponding spots are clearly separated from the GaAs ones in the power spectrum due to the high mismatch

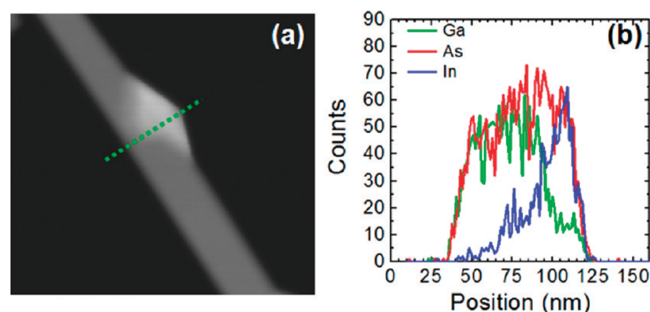

Figure 3. HAADF STEM (*Z*-contrast image) (a) and EDX line scan (b) obtained on one of the InAs QDs.

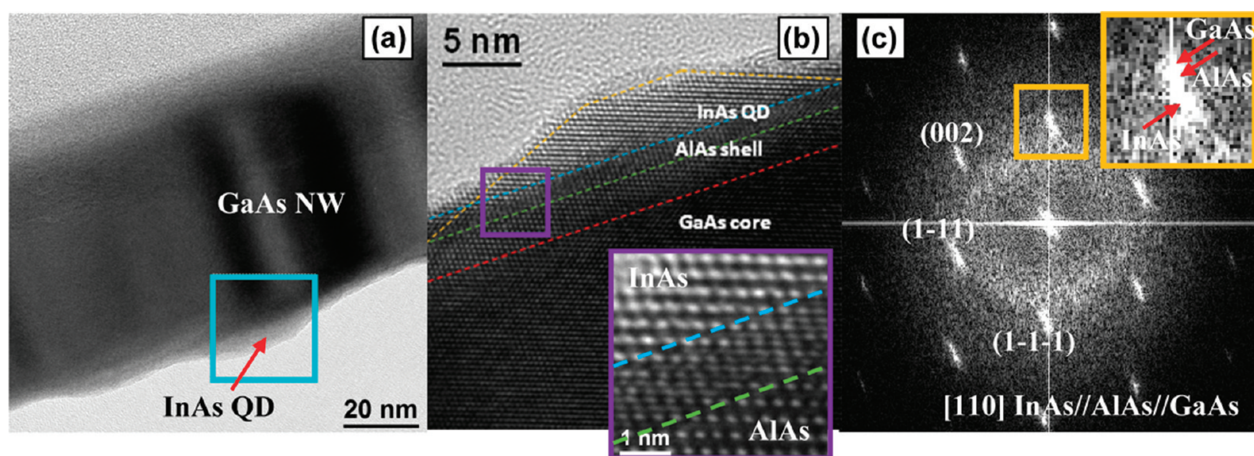

Figure 4. Transmission electron microscopy measurements of sample II: (a) QDs on the nanowire side facet (vertex) are revealed. (b) HR-TEM micrograph showing the presence of AlAs shell layer, in which the QD lies partially buried. The bottom inset shows a magnified detail of the InAs/AlAs overlapped area between the dashed lines. (c) Power spectrum (FFT) obtained on the HRTEM micrograph of panel b showing a clear splitting of the spots (the inset shows a magnified detail of the splitting).

between both materials. The non-overlap of the diffraction spots corresponding to InAs with those of AlAs/GaAs indicate that the InAs is relaxed through the formation of the QD, which is typical of the Stranski-Krastanov mechanism. We have measured the mismatch between GaAs and InAs {111} planes in the experimental micrograph above for the small QD. A value of 4.5% has been obtained, instead of the

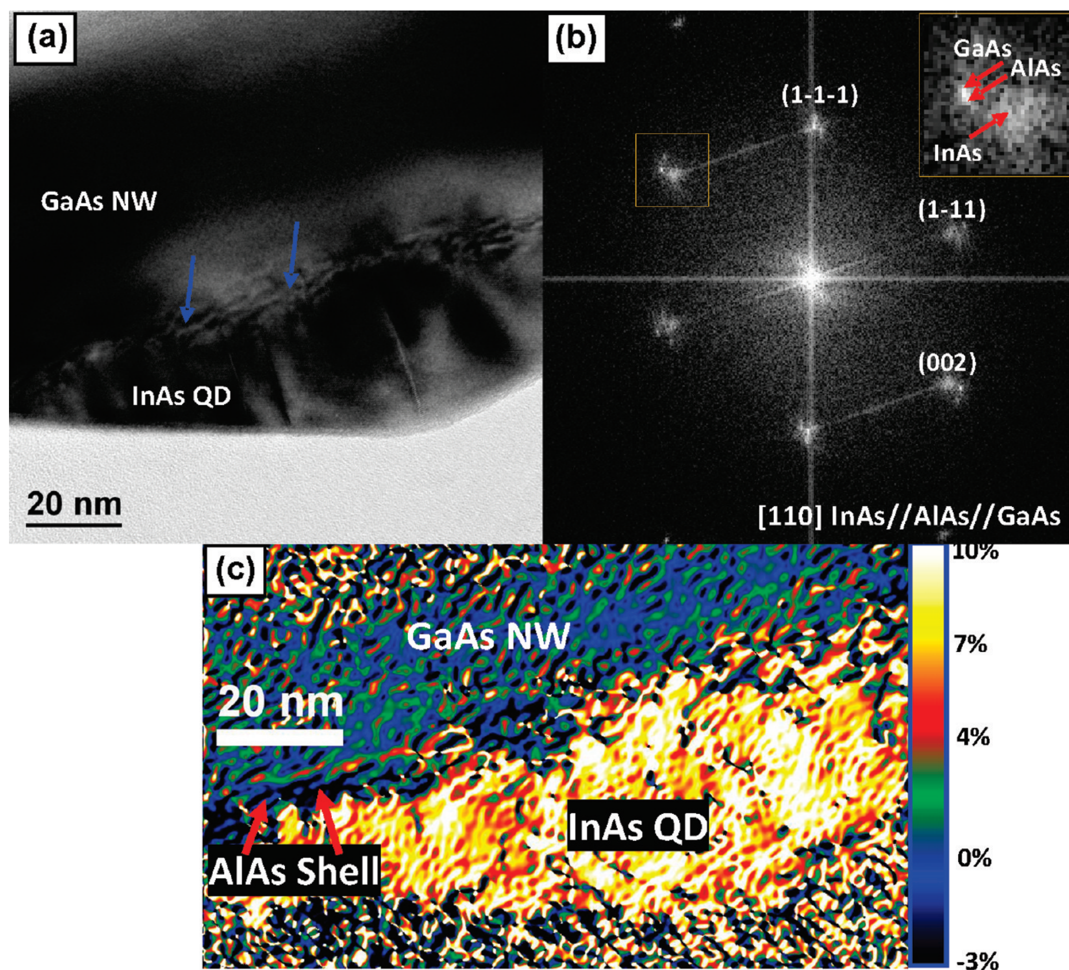

Figure 5. Transmission electron microscopy measurements of sample II: (a) detail of a larger InAs structure. The blue arrows point to the moiré fringes in the interface between the InAs and the AlAs layer which appear due to the overlapping of both structures and the difference in cell parameters; (b) Fast Fourier transform (FFT) of the image in panel a, the separation of diffractions spots and the presence of strain; and (c) geometrical phase analysis (GPA) of the image in panel a.

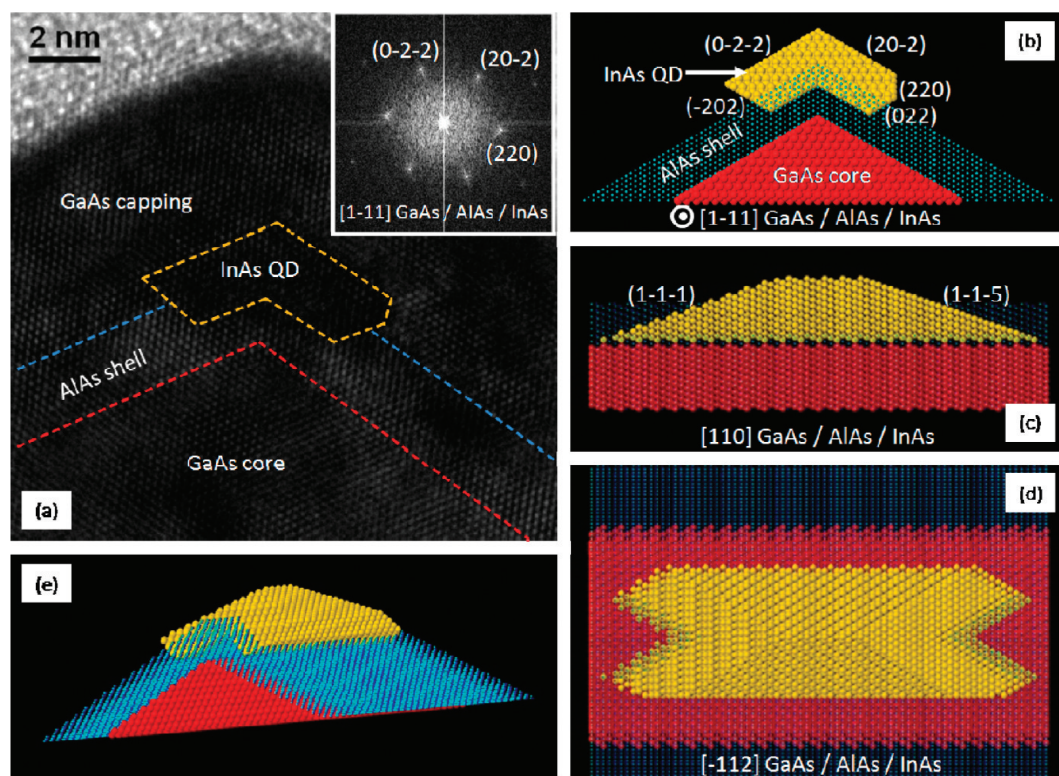

Figure 6. Cross-sectional transmission electron microscopy experiments for sample IIIc: (a) QD placed at the corner of the AlAs shell layer; power analysis in the inset. (b−e) Three-dimensional supercell model of the "corner" QD faceting, obtained by combining the information from planar view (Figure 4b) and cross-sectional HRTEM pictures (a). In the sequential order: image from the front side, from the lateral side, from the top view, and a 3D view of the model.

expected 7.2%. This means that the small InAs QDs present an in-plane compressive strain of −2.5%.

In the same sample, larger relaxed InAs islands have been observed. An example is shown in Figure 5. These islands are quite larger than the QDs, about 300−500 nm in length and 20−40 nm high. In the power spectrum of Figure 5b, a clear splitting of the spots can be observed, in agreement with the lattice mismatch. We have analyzed the fringe deformation by means of a geometrical phase analysis (GPA)[54] (Figure 5c). In the image, the GPA analysis shows that there is approximately a 7% mismatch on average between the InAs QD and the GaAs core (which has been taken as reference) and an approximate −1% mismatch between the AlAs shell and the GaAs NW core. The color map presented in Figure 5c corresponds to the GPA fringe deformation analysis obtained on the (002) spots. One should note that the strain analysis is based on the geometrical phase analysis algorithms, which take into account the FFT of the images. As a consequence of this, there are always some artifacts arising at the borders of the images. We have measured carefully the mismatch between GaAs and InAs {111} planes in the experimental micrograph above for the large QD, obtaining 7.1%, in good agreement with the expected mismatch. This experimental value corresponds to an interplanar distance for the {111} planes of 0.3496 nm instead of the 0.3498 nm expected for a bulk InAs. This last result indicates that the InAs island is technically almost fully relaxed. In order to keep a good epitaxy with the core, the only way for the InAs island is by creating mismatch or relaxation dislocations. These dislocations should appear every 15 (1−11) planes according to the calculated interplanar distances for both materials, meaning that there should be a dislocation every 5.25 nm on average. These large islands are similar to the structures observed in sample I. As observed in planar growth of InAs QDs, the presence of such large defective structures could be related to the deposition of a too thick InAs layer. It should be reduced by decreasing the amount of InAs deposited.[47] Sample III corresponds to a sample grown with the same conditions as sample II but with a much smaller InAs nominal thickness.

In order to get more insight in the nucleation mechanism, exact three-dimensional morphology and position of the InAs QDs cross-sectional HRTEM was realized. An example is shown in Figure 6a. Surprisingly, the QD does not fully lie on the nanowire side facet. It is placed at the vertex between two facets, and it is partially inserted in the AlAs shell, as already suggested in our previous lateral view HRTEM analysis (Figures 4 and 5). One should note here that with both cross-section HRTEM and AFM measurements we were able to find QDs nucleated on the corner and on the nanowire facets. We believe that the position at the corner or on the facet is favorable for a more efficient stress release,

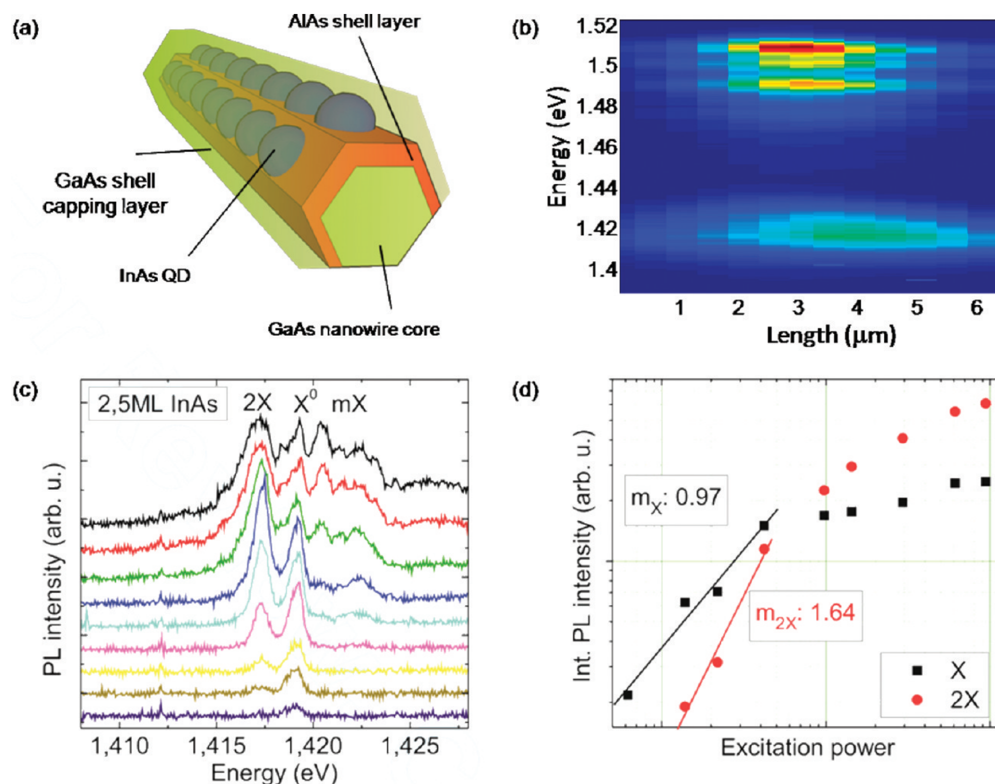

Figure 7. (a) Schematic drawing of the sample investigated by PL spectroscopy. (b) Spatial mapping of the PL along the nanowire axis. (c) Series of PL spectra obtained with increasing excitation power, showing the appearance of single, double, and multiple excitons. (d) Analysis of the integral PL signal in panel c *versus* the excitation power, with typical linear and quadratic increment for single and double exciton in QDs.

and the exact position might be a function of the facet width. Combining HRTEM measurements in planar and cross-sectional views, we were able to create a 3D supercell model for the QD. An online animation of the 3D atomic model can be found elsewhere.[55] Panels b−e of Figure 6 correspond, respectively, to a front side image along the [1−11] growth axis, a lateral side image along the [110] axis, a top view image along the [−112], and a 3D view of the model. Careful HRTEM analysis indicates that the lateral facets of the QDs correspond to {220} planes, while the front and rear facets correspond to (1−1−1) and (1−1−5) planes. The tip of the QD is parallel to the [−112] direction.

Although in HRTEM conditions the differences in contrast due to compositional changes are not extremely high, in this case, they were sufficient to delineate the different layers and the InAs QD by using typical Digital Micrograph image software. The difference in the average atomic number of the materials results in a variation of the contrast. The discontinuous lines in the HRTEM image of Figure 6a highlight the limits within the InAs, AlAs, and GaAs regions. We extrapolated a burying depth of 3−4 monolayers into the AlAs shell, corresponding approximately to 0.9−1.2 nm. This value corresponds also to the penetration depth for the dot in Figure 4b, even if in that case it was not possible to determine whether the dot was nucleated on the AlAs side facet or at the corner of AlAs layer. Therefore, we corroborate that the formation process of the QD involves the diffusion of a few monolayers of InAs in the (110) AlAs layer and that this is a fundamental phenomenon linked to the QD formation on {110} facets.

We turn now to the study of the functionality of these nanowire structures. The optical properties of the QDs were studied by confocal microphotoluminescence (PL) spectroscopy at 4.2 K. The measurements were spatially resolved on single nanowires. The PL was excited using the 632.8 nm line of a He−Ne laser and detected by the combination of a grating spectrometer and a silicon charge-coupled device (CCD). Also here, the nanowires were transferred on a silicon substrate. As mentioned above, for the optical investigations, the samples have been capped with GaAs. A schematic drawing of the sample structure is presented in Figure 7a. The spatial mapping of the luminescence collected from a nanowire corresponding to sample IIIc is shown in Figure 7b. Emission at 1.51 and 1.50 eV is observed along the nanowire. These emissions correspond to the free exciton of GaAs and to the existence of some small domains of wurtzite in the nanowire core.[56,57] Additionally, a peak at 1.415 eV is observed. Such an emission cannot be attributed to the existence of wurtzite domains or to the AlAs layer. Instead, it could be related to the emission of InAs QDs.[58,59] In order to demonstrate the QD nature of such emission, the luminescence was

recorded as a function of the excitation power. An example is reported in Figure 7c. At low excitation power, a peak at 1.419 eV with a FWHM of ~600 μeV is observed. By increasing the excitation power, the peak at 1.419 eV increases in intensity and a second one at 1.417 eV appears. Finally, for the highest excitation powers used, other peaks at energies higher than 1.42 eV appear. The analysis of the integrated intensity as a function of the excitation power is reported in Figure 7d. The intensity of the peaks at 1.419 and 1.417 eV increases, respectively, in a linear and quadratic way with the excitation power. Such a dependency enables us to attribute the two peaks to the single (X^0) and double exciton (2X or biexciton) of InAs QDs. The spectral features at higher energies are probably multiexcitonic recombination lines. The observation of typical QD behavior should only be possible provided that the QDs exhibit a high quality. These results open the way to the use of Stranski-Krastanov QD structures in nanowires for multiple optical applications.

In conclusion, we have demonstrated the fabrication of optically active Stranski-Krastanov InAs quantum dots on the facets of GaAs nanowires. For that, it is necessary to deposit an intermediate AlAs shell. The formation of the QDs has been demonstrated by atomic force and high-resolution electron microscopy. Cross-section measurements demonstrate the diffusion of the InAs QD in the AlAs shell, which has been revealed as an essential process for the QD formation. Single and biexcitions have been excited in the QDs, as shown by photoluminescence spectroscopy experiments. This in agreement with the high quality of the QD structures and opens a new avenue in the areas of nanowire-based photonics and photovoltaics.

EXPERIMENTAL SECTION

MBE Growth of Nanowires. The samples were grown in a high-purity Gen-II MBE system. In all cases, 2 in. GaAs (001)-oriented wafers covered with 35 nm thick silicon dioxide sputtered layers were used as substrates. In order to ensure a contamination-free surface, prior to introducing the substrates in the MBE, the oxide was etched down to 10 nm by dipping the substrates in a diluted buffered HF solution for 10 s (ammonium fluoride etch solution (91−9)/deionized water = 1:2). In order to desorb any remnant adsorbed molecules of the surface, the wafers were heated to 650 °C for 30 min prior to growth. During the growth, the substrate and arsenic beam flux were kept, respectively, at 630 °C and 8.8×10^{-7} mbar. The Ga source was heated at 843 °C, which corresponds to a nominal growth rate of 0.022 nm/s for planar growth under As-rich conditions. Under these conditions, 2 μm long GaAs nanowires were synthesized at a nominal growth rate of 1 μm/h. In order to grow on the nanowire facets, growth conditions were changed to As-rich conditions by increasing the As pressure up to 5×10^{-5} mbar. Without changing the substrate temperature, AlAs shells were grown with an Al growth rate equivalent to 0.011 nm/s for planar growth (1040 °C). InAs shell QDs were grown at a lower substrate temperature (465 °C) and with a very low In equivalent rate of 0.075 nm/s (770 °C). On capped samples, a GaAs shell layer was grown after the InAs QDs. The substrate was kept at 465 °C for avoiding In desorption from the QDs. Ga rate was also kept at 0.022 nm/s.

AFM Measurements. The nanowires were transferred from the original GaAs substrate on a Si substrate. The transfer was realized by sonicating the as-grown sample in an isopropyl alcohol bath and subsequently dropping the nanowire solution onto the final substrate. The AFM measurements were performed with an Asylum MFP-3D AFM system, operating in AC mode and equipped with silicon cantilevers (Olympus OMCL-AC240TS). Ultrasharp silicon cantilevers were also used. The images were analyzed both by mean of Igor Pro software, as well as by WSxM free program.[60]

HRTEM Measurements. The measurements were performed in a JEOL 2010F field emission gun microscope operated at 200 kV with a resolution of 0.19 nm. EDX scan profiles and STEM images were obtained in a JEOL 2100. The 3D supercell models were designed by using the Rhodius online software package,[61] which allows creation of complex atomic models, including nanowire-like structures with QDs or embedded nanoparticles.[62] Fringe deformation was studied by using the geometrical phase analysis (GPA).[54]

Cross-Section TEM (XTEM) Sample Preparation. High densities of parallel oriented nanowires were transferred to a silicon substrate, obtained through mechanical gentle rubbing of a piece of the as-grown substrate on a silicon substrate. A 100 nm thick SiO_2 layer was then sputtered on top of the nanowires. The cross sections perpendicular to the nanowire axis were prepared by standard TEM methods. More details on XTEM nanowire sample preparation can be found elsewhere.[37,38]

Strain Analysis. We have analyzed the fringe deformation by means of a geometrical phase analysis (GPA). The software used was the GPA package, which is running a script plug-in in the well-known GATAN Digital Micrograph. GaAs NW core was taken as a reference for the analysis, and thus the strain values are relative to GaAs. The GaAs values were based on the measured values, with excellent agreement with the literature values. In order to obtain the strain values for InAs, we calculated the average value in an area comprising the center of the QD. Due to the morphology of the QD (several facets are included as shown in the models), it is clear that thickness and internal strains may change slightly along the QD, this can be the reason, as well as the presence of dislocations and partial relaxations.

Acknowledgment. The authors thank G. Abstreiter, T. Garma, and M. Bichler for their experimental support and discussions. This research was supported by Marie Curie Excellence Grant "SENFED", the DFG excellence cluster Nanosystems Initiative Munich, as well as SFB 631 and European Research Council Starting Grant "Upcon". This work was partially supported by the Spanish Government projects Consolider Ingenio 2010 CSD2009 00013 IMAGINE and CSD2009 00050 MULTICAT. J.A. acknowledges the funding from the Spanish CSIC project NEAMAN and the MICINN project MAT2010-15138 (COPEON). The authors would like to thank the TEM facilities in Serveis Cientificotècnics from Universitat de Barcelona.

Supporting Information Available: Additional analysis on the cross-section analysis of the samples and the interdiffusion of InAs in the AlAs layer. This material is available free of charge *via* the Internet at http://pubs.acs.org.

REFERENCES AND NOTES

1. Wang, W. U.; Chen, C.; Lin, K. H.; Fang, Y.; Lieber, C. M. Label-Free Detection of Small-Molecule−Protein Interactions by Using Nanowire Nanosensors. *Proc. Natl. Acad. Sci. U.S.A.* **2005**, *102*, 3208–3212.
2. Zheng, G. F.; Patolsky, F.; Cui, Y.; Wang, W. U.; Lieber, C. M. Multiplexed Electrical Detection of Cancer Markers with Nanowire Sensor Arrays. *Nat. Biotechnol.* **2005**, *23*, 1294–1301.
3. Cui, Y.; Lieber, C. M. Functional Nanoscale Electronic Devices Assembled Using Silicon Nanowire Building Blocks. *Science* **2001**, *291*, 851–853.

4. Duan, X. F.; Huang, Y.; Cui, Y.; Wang, J. F.; Lieber, C. M. Indium Phosphide Nanowires as Building Blocks for Nanoscale Electronic and Optoelectronic Devices. *Nature* **2001**, *409*, 66–69.
5. Cui, Y.; Zhong, Z. H.; Wang, D. L.; Wang, W. U.; Lieber, C. M. High Performance Silicon Nanowire Field Effect Transistors. *Nano Lett.* **2003**, *3*, 149–152.
6. Chan, C. K.; Peng, H.; Liu, G.; McIlwrath, K.; Zhang, X. F.; Huggins, R. A.; Cui, Y. High-Performance Lithium Battery Anodes Using Silicon Nanowires. *Nat. Nanotechnol.* **2008**, *3*, 31–33.
7. Chan, C. K.; Zhang, X. F.; Cui, Y. High Capacity Li Ion Battery Anodes Using Ge Nanowires. *Nano Lett.* **2008**, *8*, 307–309.
8. Kayes, B. M.; Atwater, H. A.; Lewis, N. S. Comparison of the Device Physics Principles of Planar and Radial p−n Junction Nanorod Solar Cells. *J. Appl. Phys.* **2005**, *97*, 114302.
9. Tian, B. Z.; Zheng, X. L.; Kempa, T. J.; Fang, Y.; Yu, N. F.; Yu, G. H.; Huang, J. L.; Lieber, C. M. Coaxial Silicon Nanowires as Solar Cells and Nanoelectronic Power Sources. *Nature* **2007**, *449*, 885–888.
10. Hochbaum, A. I.; Chen, R. K.; Delgado, R. D.; Liang, W. J.; Garnett, E. C.; Najarian, M.; Majumdar, A.; Yang, P. D. Enhanced Thermoelectric Performance of Rough Silicon Nanowires. *Nature* **2008**, *451*, 163–165.
11. Boukai, A. I.; Bunimovich, Y.; Tahir-Kheli, J.; Yu, J. K.; Goddard, W. A.; Heath, J. R. Silicon Nanowires as Efficient Thermoelectric Materials. *Nature* **2008**, *451*, 168–165.
12. Thelander, C.; Martensson, T.; Bjork, M. T.; Ohlsson, B. J.; Larsson, M. W.; Wallenberg, L. R.; Samuelson, L. Single-Electron Transistors in Heterostructure Nanowires. *Appl. Phys. Lett.* **2003**, *83*, 2052–2055.
13. Pfund, A.; Shorubalko, I.; Ensslin, K.; Leturcq, R. Suppression of Spin Relaxation in an InAs Nanowire Double Quantum Dot. *Phys. Rev. Lett.* **2007**, *99*, 036801.
14. van Weert, M. H. M.; Akopian, N.; Perinetti, U.; van Kouwen, M. P.; Algra, R. E.; Veheijen, M. A.; Bakkers, E. P. A. M.; Kouwenhoven, L. P.; Zwiller, V. Selective Excitation and Detection of Spin States in a Single Nanowire Quantum Dot. *Nano Lett.* **2009**, *9*, 1989–1993.
15. Doh, Y. J.; van Dam, J. A.; Roest, A. L.; Bakkers, E. P. A. M.; Kouwenhoven, L. P.; De Franceschi, S. Tunable Supercurrent through Semiconductor Nanowires. *Science* **2005**, *309*, 272–275.
16. Skold, N.; Karlsson, L. S.; Larsson, M. W.; Pistol, M. E.; Seifert, W.; Tragardh, J.; Samuelson, L. Growth and Optical Properties of Strained GaAs-$Ga_xIn_{1-x}P$ Core−Shell Nanowires. *Nano Lett.* **2005**, *5*, 1943–1947.
17. Gudiksen, M. S.; Lauhon, L. J.; Wang, J.; Smith, D. C.; Lieber, C. M. Growth of Nanowire Superlattice Structures for Nanoscale Photonics and Electronics. *Nature* **2002**, *415*, 617–620.
18. Johnson, J. C.; Yan, H. Q.; Yang, P. D.; Saykally, R. J. Optical Cavity Effects in ZnO Nanowire Lasers and Waveguides. *J. Phys. Chem. B* **2003**, *107*, 8816–8828.
19. Zimmler, M. A.; Stichtenoth, D.; Ronning, C.; Yi, W.; Narayanamurti, W.; Voss, T.; Capasso, F. Scalable Fabrication of Nanowire Photonic and Electronic Circuits using Spin-on Glass. *Nano Lett.* **2008**, *8*, 1695–1699.
20. Borgström, M. T.; Zwiller, V.; Mueller, E.; Imamoglu, A. Optically Bright Quantum Dots in Single Nanowires. *Nano Lett.* **2005**, *5*, 1439–1443.
21. Björk, M. T.; Ohlsson, B. J.; Sass, T.; Persson, A. I.; Thelander, C.; Magnusson, M. H.; Deppert, K.; Wallenberg, L. R.; Samuelson, L. One-Dmensional Steeplechase for Electrons Realized. *Nano Lett.* **2002**, *2*, 87–89.
22. Pfund, A.; Shorubalko, I.; Leturcq, R.; Ensslin, K. Top-Gate Defined Double Quantum Dots in InAs Nanowires. *Appl. Phys. Lett.* **2006**, *89*, 252106.
23. Minot, E. D.; Kelkensberg, F.; van Kouwen, M.; van Dam, J. A.; Kouwenhoven, L. P.; Zwiller, V.; Borgström, M. T.; Wunnicke, O.; Verheijen, M. A.; Bakkers, E. P. A. M. Single Quantum Dot Nanowire LEDs. *Nano Lett.* **2007**, *7*, 367–370.
24. Leschkies, K. S.; Jacobs, A. G.; Norris, D. J.; Aydil, E. S. Nanowire-Quantum-Dot Solar Cells and the Influence of Nanowire Length on the Charge Collection Efficiency. *Appl. Phys. Lett.* **2009**, *95*, 193103–193105.
25. Colombo, C.; Heiss, M.; Graetzel, M.; Fontcuberta i Morral, A. Gallium Arsenide p-i-n Radial Structures for Photovoltaic Applications. *Appl. Phys. Lett.* **2009**, *94*, 173108–173111.
26. Kelzenberg, M. D.; Boettcher, S. W.; Petykiewicz, J. A.; Turner-Evans, D. B.; Putnam, M. C.; Warren, E. L.; Spurgeon, J. M.; Briggs, R. M.; Lewis, N. S.; Atwater, H. A. Enhanced Absorption and Carrier Collection in Si Wire Arrays for Photovoltaic Applications. *Nat. Mater.* **2010**, *9*, 239–244.
27. Wagner, R. S.; Ellis, W. C. Vapor−Liquid−Solid Mechanism of Single Crystal Growth. *Appl. Phys. Lett.* **1964**, *4*, 89–91.
28. Hiruma, K.; Murakoshi, H.; Yazawa, M.; Katsuyama, T. Self-Organized Growth of GaAs/InAs Heterostructure Nanocylinders by Organometallic Vapor Phase Epitaxy. *J. Cryst. Growth* **1996**, *163*, 226–231.
29. Wu, Y.; Fan, R.; Yang, P. Block-by-Block Growth of Single-Crystalline Si/SiGe Superlattice. Nanowires. *Nano Lett.* **2002**, *2*, 83–86.
30. Li, D. Y.; Wu, Y.; Fan, R.; Yang, P. D.; Majumdar, A. Thermal Conductivity of Si/SiGe Superlattice Nanowires. *Appl. Phys. Lett.* **2003**, *83*, 3186–3188.
31. Bjork, M. T.; Thelander, C.; Hansen, A. E.; Jensen, L. E.; Larsson, M. W.; Wallenberg, L. R.; Samuelson, L. Few-Electron Quantum Dots in Nanowires. *Nano Lett.* **2004**, *4*, 1621–1625.
32. Heiss, M.; Gustafsson, A.; Conesa-Boj, S.; Peiro, F.; Morante, J. R.; Abstreiter, G.; Arbiol, J.; Samuelson, L.; Fontcuberta i Morral, A. Catalyst-Free Nanowires with Axial $In_xGa_{1-x}As$/GaAs Heterostructures. *Nanotechnology* **2009**, *20*, 075603.
33. Ouattara, L.; Mikkelsen, A.; Sköld, N.; Eriksson, J.; Knaapen, T.; Æavar, E.; Seifert, W.; Samuelson, L.; Lundgren, E. GaAs/AlGaAs Nanowire Heterostructures Studied by Scanning Tunneling Microscopy. *Nano Lett.* **2007**, *7*, 2859–2864.
34. Dick, K. A.; Kodambaka, S.; Reuter, M. C.; Deppert, K.; Samuelson, L.; Seifert, W.; Wallenberg, L. R.; Ross, F. M. The Morphology of Axial and Branched Nanowire Heterostructures. *Nano Lett.* **2007**, *7*, 1817–1822.
35. Stranski, I. N.; Von Krastanow, L. Abhandlungen der Mathematisch-Naturwissenschaftlichen Klasse. *Akademie der Wissenschaften und der Literatur in Mainz* **1939**, *146*, 797.
36. Paladugu, M.; Zou, J.; Guo, Y. N.; Zhang, X.; Joyce, H. J.; Gao, Q.; Tan, H. H.; Jagadish, C.; Kim, Y. Formation of Hierarchical InAs Nanoring/GaAs Nanowire Heterostructures. *Angew. Chem.* **2009**, *48*, 780–783.
37. Fontcuberta i Morral, A.; Spirkoska, D.; Arbiol, J.; Heigoldt, M.; Morante, J. R.; Abstreiter, G. Prismatic Quantum Heterostructures Synthesized on Molecular-Beam Epitaxy GaAs Nanowires. *Small* **2008**, *4*, 899–903.
38. Heigoldt, M.; Arbiol, J.; Spirkoska, D.; Rebled, J. M.; Conesa-Boj, S.; Abstreiter, G.; Peiro, F.; Morante, J. R.; Fontcuberta i Morral, A. Long Range Epitaxial Growth of Prismatic Heterostructures on the Facets of Catalyst-Free GaAs Nanowires. *J. Mater. Chem.* **2009**, *19*, 840–848.
39. Arbiol, J.; Fontcuberta i Morral, A.; Estradé, S.; Peiró, F.; Kalache, B.; Roca i Cabarrocas, P.; Morante, J. R. Influence of the (111) Twinning on the Formation of Diamond Cubic/Diamond Hexagonal Heterostructures in Cu-Catalyzed Si Nanowires. *J. Appl. Phys.* **2008**, *104*, 064312-5.
40. Czaban, J. A.; Thompson, D. A.; LaPierre, R. R. GaAs Core−Shell Nanowires for Photovoltaic Applications. *Nano Lett* **2009**, *9*, 148–154.
41. Joyce, P. B.; Krzyzewski, T. J.; Bell, G. R.; Joyce, B. A.; Jones, T. S. Composition of InAs Quantum Dots on GaAs(001): Direct Evidence for (In, Ga)As Alloying. *Phys. Rev. B* **1998**, *58*, R15981.
42. Leonard, D.; Pond, K.; Petroff, P. M. Critical Layer Thickness for Self-Assembled InAs Islands on GaAs. *Phys. Rev. B* **1994**, *50*, 11687–11692.
43. Belk, J. G.; Pashley, D. W.; McConville, C. F.; Sudijono, J. L.;

Joyce, B. A.; Jones, T. S. Surface Atomic Configurations Due to Dislocation Activity in InAs/GaAs(110) Heteroepitaxy. *Phys. Rev. B* **1997**, *56*, 10289–10296.
44. Joyce, B. A.; Sudijono, J. L.; Belk, J. G.; Yamaguchi, H.; Zhang, X. M.; Dobbs, H. T.; Zangwill, A.; Vvedensky, D. D.; Jones, T. S. A Scanning Tunneling Microscopy Reflection High Energy Electron Diffraction-Rate Equation Study of the Molecular Beam Epitaxial Growth of InAs on GaAs(001), (110) and (111)A—Quantum Dots and Two-Dimensional Modes. *Jpn. J. Appl. Phys. Part 1* **1997**, *36*, 4111–4117.
45. Yoshita, M.; Akiyama, H.; Pfeiffer, L. N.; West, K. W. Quantum Wells with Atomically Smooth Interfaces. *Appl. Phys. Lett.* **2002**, *81*, 49–51.
46. Wasserman, D.; Lyon, S. A.; Hadjipanayi, M.; Maciel, A.; Ryan, J. F. Formation of Self-Assembled InAs Quantum Dots on (110) GaAs Substrates. *Appl. Phys. Lett.* **2003**, *83*, 5050–5052.
47. Uccelli, E.; Bichler, M.; Nürnberger, S.; Abstreiter, G.; Fontcuberta i Morral, A. Controlled Synthesis of InAs Wires, Dot and Twin-Dot Array Configurations by Cleaved Edge Overgrowth. *Nanotechnology* **2008**, *19*, 045303.
48. Uccelli, E.; Nürnberger, S.; Bichler, M.; Abstreiter, G.; Fontcuberta i Morral, A. Growth Mechanisms of Self-Assembled InAs Quantum Dots on (110) AlAs/GaAs Cleaved Facets. *Superlattices Microstruct.* **2008**, *44*, 425–430.
49. Niu, X. B.; Uccelli, E.; Fontcuberta i Morral, A.; Ratsch, C. A Level Set Simulation for Ordering of Quantum Dots *via* Cleaved-Edge Overgrowth. *Appl. Phys. Lett.* **2009**, *95*, 023119–023121.
50. Colombo, C.; Spirkoska, D.; Frimmer, M.; Abstreiter, G.; Fontcuberta i Morral, A. Ga-Assisted Catalyst-Free Growth Mechanism of GaAs Nanowires by Molecular Beam Epitaxy. *Phys. Rev. B* **2008**, *77*, 155326.
51. Fontcuberta i Morral, A.; Colombo, C.; Arbiol, J.; Morante, J. R.; Abstreiter, G. Nucleation Mechanism of Gallium-Assisted Molecular Beam Epitaxy Growth of Gallium Arsenide Nanowires. *Appl. Phys. Lett.* **2008**, *92*, 063112-4.
52. Lobo, C.; Leon, R. InGaAs Island Shapes and Adatom Migration Behavior on (100), (110), (111), and (311) GaAs Surfaces. *J. Appl. Phys.* **1998**, *83*, 4168–4172.
53. Fontcuberta i Morral, A.; Arbiol, J.; Prades, J. D.; Cirera, A.; Morante, J. R. Synthesis of Silicon Nanowires with Wurtzite Crystalline Structure by Using Standard Chemical Vapor Deposition. *Adv. Mater.* **2007**, *19*, 1347.
54. Hÿtch, M. J.; Snoeck, E.; Kilaas, R. Quantitative Measurement of Displacement and Strain Fields from HREM Micrographs. *Ultramicroscopy* **1998**, *74*, 131–146.
55. http://www.icmab.es/gaen/research/121.html.
56. Spirkoska, D.; Colombo, C.; Heiss, M.; Abstreiter, G.; Fontcuberta i Morral, A. The Use of Molecular Beam Epitaxy for the Synthesis of High Purity III−V Nanowires. *J. Phys.: Condens. Matter.* **2008**, *20*, 454225.
57. Spirkoska, D.; Ariol, J.; Gustafsson, A.; Conesa-Boj, S.; Glas, F.; Zardo, I.; Heigoldt, M.; Gass, M. H.; Bleloch, A. L.; Estrade, S.; Kaniber, M.; Rossler, J.; Peiro, F.; Morante, J. R.; Abstreiter, G.; Samuelson, L.; Fontcuberta i Morral, A. Structural and Optical Properties of High Quality Zinc-Blende/Wurtzite GaAs Nanowire Heterostructures. *Phys. Rev. B* **2009**, *80*, 245325.
58. Uccelli, E.; Waller, L.; Bichler, M.; Abstreiter, G.; Fontcuberta i Morral, A. Optical Properties of InAs Quantum Dot Array Ensembles with Predetermined Lateral Sizes from 20 to 40 nm. *Jpn. J. Appl. Phys.* **2010**, *49*, 045201.
59. Bauer, J.; Schuh, D.; Uccelli, E.; Schulz, R.; Kress, A.; Hofbauer, F.; Finley, J. J.; Abstreiter, G. Long-Range Ordered Self-Assembled InAs Quantum Dots Epitaxially Grown on (110) GaAs. *Appl. Phys. Lett.* **2004**, *85*, 4750.
60. Horcas, I.; Fernández, R.; Gómez-Rodríguez, J. M.; Colchero, J.; Gómez-Herrero, J.; Baro, A. M. WSXM: A Software for Scanning Probe Microscopy and a Tool for Nanotechnology. *Rev. Sci. Instrum.* **2007**, *78*, 013705.
61. Bernal, S.; Botana, F. J.; Calvino, J. J.; López Cartes, C.; Pérez Omil, J. A.; Rodríguez-Izquierdo, J. M. The Interpretation of HREM Images of Supported Metal Catalysts Using Image Simulation: Profile View Images. *Ultramicroscopy* **1998**, *72*, 135–164.
62. Arbiol, J.; Cirera, A.; Peiró, F.; Cornet, A.; Morante, J. R.; Delgado, J. J.; Calvino, J. J. Optimization of Tin Dioxide Nanosticks Faceting for the Improvement of Palladium Nanocluster Epitaxy. *Appl. Phys. Lett.* **2002**, *80*, 329–331.